Gravity inversion in a user-friendly environment

João B. C. Silva(*), UFPA, and Valeria C. F. Barbosa, LNCC.

Abstract

In a user-friendly environment we present a method for inverting gravity data produced by multiple, complex and interfering 2D gravity sources having arbitrary shapes and arbitrary, but known density contrast. Our method is stable and is suitable to recover a complex 2D density distribution, leading to a reliable delineation of sectionally homogeneous sources with complex shapes. It is a method similar to interactive modeling but differs from it in automatically fitting the observations and in requiring from the interpreter only the knowledge of the outlines of the sources expressed by simple geometric elements such as points and line segments. Each geometric element operates as a skeletal outline of a particular homogeneous section of the gravity source to be reconstructed. Also, the interpreter can define the geometric elements in an interactive way without worrying about the data fitting because it is automatically done. The examples with synthetic data illustrate the good performance of the method in mapping the complex geometry of gravity sources. The solution sensitivity to uncertainties in the prior information shows that to produce good results, the uncertainty on the contrast density of each homogeneous extent of the source should be smaller than 40 percent. The method was also applied to two sets of real data. The first one consists of several positive anomalies produced by metabasalts and metagabbros from a greenstone belt located in Rio Maria region, in Pará state, Brazil. The second one is a negative gravity anomaly produced by the Bodmin Moor Granite, which is part of the Cornubian Batholith in southwestern England. The estimated density contrast distribution in all tests demonstrates a good correlation of the estimated gravity sources with corresponding known geological features.

Introduction

The presented method is based on Guillen and Menichetti's (1984) inversion procedure modified to permit the interpretation of anomalies caused by complex and interfering sources. The modification consists in extending the procedure for several sources and in allowing different density contrasts to be assigned to each presumed sources (we use the term *presumed sources* to describe the sources which the interpreter assumes to exist). With this facility, multiple, complex and laterally interfering sources with different density contrasts can be easy and quickly delineated.

Method

Let S_r , $r = 1,..., R$, be a set of 2D gravity sources having arbitrary shapes and arbitrary density contrast distribution and assume that outlines of these sources may be constructed by a combination of axes and points, totaling L geometric elements (Figure 1). Let T be the set of all geometric elements, e_i , $i = 1,..., L$ (points and axes), ordered in an arbitrary way. Each element, e_i , of T is assigned a target density contrast. Additionally, we assign to the *j*th source a subset, t_j , of T containing K_j geometric elements and K_j target density contrasts. By combining *i*) the presumably known sources outline (axes and points), *ii*) the corresponding target density contrasts, and *iii*) the measurements of the gravity anomaly produced by the R sources, we proceed at improving the source delineation. To this end, first assume an interpretation model consisting of an $N_x \times N_z$ grid of 2D vertical juxtaposed prisms (Figure 1), whose density contrasts are the only unknown parameters. The gravity anomaly, $g_i \equiv g(x_i)$, produced by such interpretation model at $x = x_i$ is given by

$$g_i = \sum_{j=1}^{M} p_j A_{ij} \ , \quad i = 1, 2 \ldots N \ , \tag{1}$$

where A_{ij} is numerically equal to the gravity anomaly produced at x_i by the *j*th prism, with unit density contrast, N is the number of observations, M is the total number of prisms, and $\mathbf{p}$ is an $M \times 1$ vector of unknowns whose element, p_j , is the density contrast of the *j*th prism.

Using matrix notation, equation (1) becomes

$$\mathbf{g} = \mathbf{A}\mathbf{p} \ . \tag{2}$$

To obtain a stable solution of the linear system (2), we look for the solution satisfying the gravity anomaly and presenting most of its mass excess (or deficiency) concentrated about the specified geometric elements. This is accomplished by generalizing the iterative approach by Guillen and Menichetti (1984), which consists in the following steps. First, obtain a standard minimum norm solution

$$\hat{\mathbf{p}}^{o} = \mathbf{A}^T (\mathbf{A}\mathbf{A}^T + \mu \mathbf{I})^{-1} \mathbf{g} \ , \tag{3}$$

where μ is a non-negative scalar. The larger the value of μ, the smaller the Euclidean norm of $\hat{\mathbf{p}}^{o}$. Then, the parameter estimate is iteratively updated by

$$\hat{\mathbf{p}}^{(k+1)} = \hat{\mathbf{p}}_F^{(k)} + \Delta\mathbf{p}^{(k)}, \quad (4)$$

where

$$\Delta\mathbf{p}^{(k)} = \mathbf{W}_k^{-1}\mathbf{A}^T(\mathbf{A}\mathbf{W}_k^{-1}\mathbf{A}^T + \mu\,\mathbf{I})^{-1}\left(\mathbf{g} - \mathbf{A}\hat{\mathbf{p}}_F^{(k)}\right), \quad (5)$$

$\mathbf{W}_k$ is a diagonal matrix whose nonzero elements are given by

$$w_{jj} = \frac{d_j^2}{\left|\hat{p}_j^{(k)}\right| + \varepsilon}, \quad (6)$$

$$d_j = \min_{1 < i < L} d_{ij}, \quad (7)$$

and d_{ij} is the distance from the center of the jth elementary prism to the ith geometric element. The elements of vector $\hat{\mathbf{p}}_F^{(k)}$ are either elements of vector $\hat{\mathbf{p}}^{(k)}$ or "frozen" parameters obtained by the procedure described in next paragraph. Parameter μ favors solutions in which the elementary prisms lying in the neighborhood of the geometric elements are assigned the largest density contrasts estimates in absolute values. So, the larger μ, the closer to the geometric elements will be the estimated sources. This parameter also controls the stability of the solutions. The larger μ, the more stable is the solution. An optimum value for μ is the smallest positive value still producing stable solutions. Alternatively, if the interpreter has a great confidence on the assumed outline of the true sources, μ should be the largest positive value still producing an acceptable fit to the data. The stability of a solution is verified by contaminating the data with different sequences of pseudorandom noise realizations and checking whether all estimates are computed within an acceptable precision. Matrix $\mathbf{W}_k$ controls the modulus of the correction, $\Delta\mathbf{p}^{(k)}$, at each iteration.

Cells close to any geometric element and having large density contrast estimates (in the modulus) at the previous iteration are assigned a small weight, so, the corresponding corrections may be large. Conversely, cells far from all geometric elements and having small density contrast estimates (in the modulus) at the previous iteration are assigned a large weight, so the corrections will be small. In this way, the solutions will be biased toward a concentration of the excess (or deficiency) of mass close to the geometric elements.

The above procedure, if unchecked, will produce an enormous mass concentration (or deficiency) about the geometric elements, so unrealistic density contrast estimates may show up. To constrain these estimates to geologically meaningful ranges and at the same time to impose density contrast homogeneity about the geometric elements, the following procedure is added to the algorithm.

An M-dimensional vector, $\mathbf{v}$, is defined whose jth element, v_j, is the target density contrast to be assigned to the jth cell in the following way. If the projection of the jth cell on each axis lies outside the respective axis segment, then v_j is set to zero; otherwise, it is assigned the target density contrast ascribed to the geometric element closest to the jth cell. If at the kth iteration, an estimate $\hat{p}_j^{(k)}$ lies outside the interval [0, v_j] for positive density contrasts, or the interval [v_j, 0] for negative density contrasts, then jth element of $\hat{\mathbf{p}}_F^{(k)}$ is replaced by the violated boundary (0 or v_j) and the corresponding weight, w_{jj}, is assigned a relatively large value, f, to impose the condition that the density contrast estimate at the cell be at least temporarily frozen at the violated boundary.

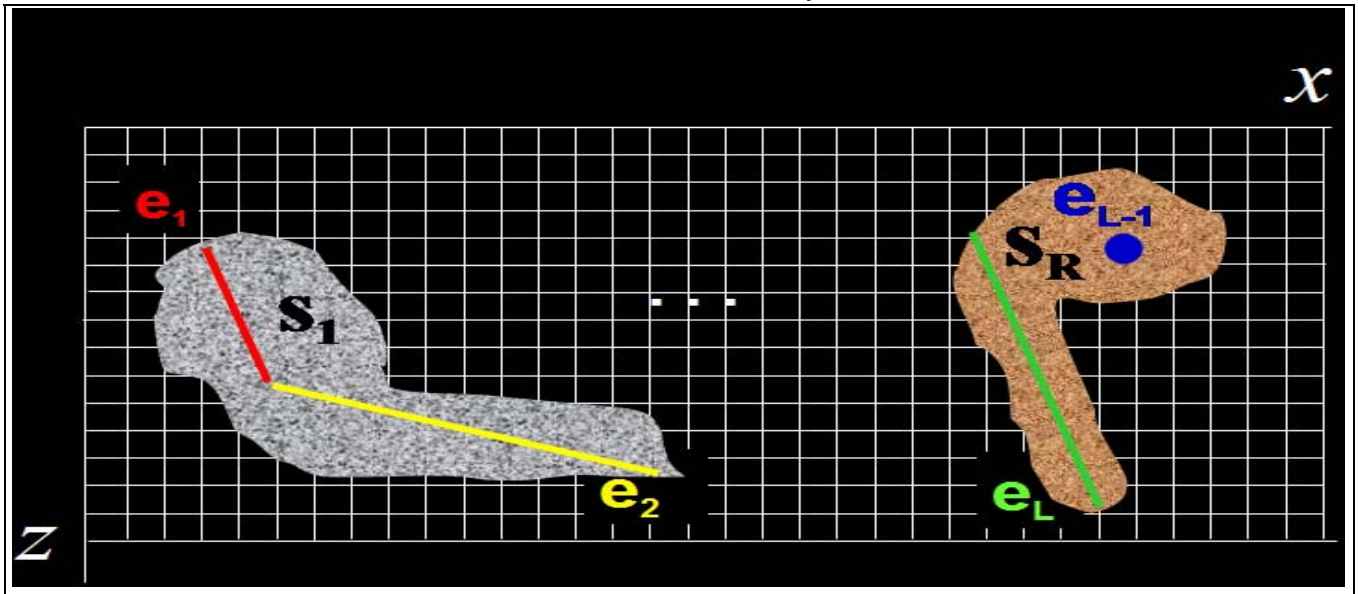

Figure 1 – Interpretation model consisting of a set of 2D vertical juxtaposed prisms, whose density contrasts are the parameters to be estimated. Anomalous sources S_r, $r = 1,..., R$, whose outlines are defined from a set of L presumably known geometric elements (axes and points), e_i, $i = 1,..., L$.

If $\hat{p}_j^{(k)}$ lies within the prescribed boundaries, the jth element of $\hat{\mathbf{p}}_F^{(k)}$ is not modified (i.e., is equal a $\hat{p}_j^{(k)}$) and the corresponding weight is computed normally by equation (6). A large value assigned to f tends to maintain the frozen density contrast estimates along the iteration. In practice, the need to increase the value of f is signaled by the occurrence of estimated sources displaying the maximum density contrasts approximately constant and greater (in absolute value) than the target density contrast at the final iterations. On the other hand, if the convergence to the specified target contrast occurs monotonically along the iteration, acceptable values assigned to f may differ by several orders of magnitude without producing appreciable changes in the final result. The nonlinearity of matrix $\mathbf{W}_k$ determines that the inverse gravity problem is nonlinear and must be solved iteratively. Despite this nonlinearity, any intermediate solutions obtained at every iteration through equations (4) and (5) fit the data within the measurement precision. This occurs because of the method's particularities described below. The first iteration is a standard minimum norm solution which fits the data. Subsequent iterations firstly modify the current solution approximation by freezing some parameters at the violated bound. As a result, this modified parameter approximation [$\hat{\mathbf{p}}_F^{(k)}$ in equation (4)] does not fit the observations. Secondly, the parameter vector necessary to explain the residual between the observations and the fitting produced by $\hat{\mathbf{p}}_F^{(k)}$ is computed [$\Delta\mathbf{p}^{(k)}$ in equation (5)]. Finally, this vector is added to $\hat{\mathbf{p}}_F^{(k)}$ [equation (4)] producing $\hat{\mathbf{p}}^{(k+1)}$, which will evidently fit the observations. We stress that the iterative procedure is needed because along the first iterations, despite the acceptable fit, the solutions are not yet sufficiently concentrated about the specified geometric elements, that is, the a priori information has not been fully introduced.

No explicit starting approximation is necessary for vector $\mathbf{p}$. The iteration is initialized simply by setting w_{jj} =1 in equation (5), but the final solution is not sensitive to this approximation and any other set of values may in theory be used to initialize w_{jj}. In practice, some numerical Problems may occur if values assigned to w_{jj} for different indices j differ from each other by several orders of magnitude. The iteration is stopped when

$$\hat{p}_j^{(k)} \le (1+\tau)\cdot v_j, \quad j = 1,\cdots M \ , \qquad (8)$$

where τ is a positive scalar controlling the degree of homogeneity assumed for the estimated sources. The larger the value of τ, the greater the homogeneity. A typical value is 0.01, corresponding to a source with density contrast variation equal or less than 1 percent of the target density contrast. The stopping criteria is based only on the estimated density contrasts because, as mentioned before, at all iterations the fitted anomaly explains the observations within the measurement precision.

Synthetic Gravity Data Produced by Separate Laterally Interfering Sources

To illustrate the utility of the present approach in interactive inversion of gravity profiles caused by interfering sources with complex shapes, we modeled three salt canopies with roots having density contrast of –0.2 g/cm^3. The interpretation model consists of a grid of 160 $\times$ 64 cells with dimensions of 0.125 km and 0.125 km in the $x-$ and $z-$ directions, respectively, and the inversion parameter are: μ = 0.2, f = 50000, and τ = 0.01. The anomaly was contaminated with pseudorandom Gaussian noise with zero mean and standard deviation of 0.1 mGal. All steps, from the design of the simulated source, the specification of the parameters related to the noise contamination of the anomaly, to the input of the geometric elements, and the choice of the inversion parameters are done interactively in a user-friendly environment. Figure 2 shows the output screen for this test. Figure 2a shows the observed and fitted anomalies (black crosses and solid blue line, respectively). Figure 2b shows the true sources in solid black lines, the axes defining the sources outline in green, and the inverted density contrasts, mapped according to the color bar. The target density contrasts assigned to all axes are equal to –0.2 g/cm^3. It can be seen that the observations are fitted within the measurement errors and the estimated sources are close to the true one because the specified geometric elements reflect factual geometric attributes of the true sources.

Tests with Real Data

Rio Maria Greenstone Belt - Figure 3a shows, in red line, a gravity profile across a greenstone belt consisting of meta-volcano sedimentary rocks in Rio Maria region, state of Pará, Brazil. This unit was compressed by two blocks of granitoid rocks in a dextral transpression regimen (Souza et al., 1992). Density measurements of rock samples collected from outcrops indicate that the density contrast between the meta-volcano sedimentary and the granitoid rocks is about 0.3 g/cm^3. Figure 3a shows the fitted gravity anomaly (blue line) produced by Souza et al.'s (1992) interpretation (Figure 3b) using interactive gravity modeling based on the expected synformal geometry for the greenstone belt unit and assigning uniform density contrasts of 0.3 g/cm^3, 0.32 g/cm^3, and 0.32 g/cm^3 to sources A, B, and C, respectively. We inverted the same anomaly assuming an interpretation model consisting of a grid of 72 $\times$ 64 cells with dimensions of 0.5 km 0.125 km in the $x-$ and $z-$ directions, respectively. We set μ = 0.05, f = 50000, and τ = 0.05. Figure 4 shows the output screen for this test. The geometric elements (axes and points in Figure 4b) were defined so as to produce estimated sources as close as possible to the interpretation given in Figure 3b. All geometric elements were assigned a target density contrast of 0.3 g/cm^3. The result (Figure 4b) shows that the proposed approach may lead to interpretations of multiple and complex sources equivalent to the ones obtained by interactive modeling, but in a much easier and faster way and with the certainty of obtaining an

acceptable fit to the data, as shown in Figure 4a (red line).

Cornubian Batholith - Figure 5a shows the gravity anomaly (blue dots) produced by the Bodmin Moor pluton, which is part of the Cornubian Batholith located in the county of Cornwall, England. The batholith has a granitic composition and intrudes low-grade, regionally metamorphosed sediments and igneous rocks. Bott and Scott (1964) modeled this pluton by incorporating the assumption that its density contrast increases to the north via a model consisting of three homogeneous compartments with density contrasts of –0.16 g/cm^3 (the southernmost), -0.13 g/cm^3 (the intermediate), and –0.10 g/cm^3 (the northernmost). Bott and Scott's (1964) interpretation and the correspondent fitted gravity anomaly are shown in Figures 5b (solid red line) and 5a (dashed red line), respectively.

We inverted this anomaly by assuming an interpretation model consisting of 58 $\times$ 24 cells with dimensions of 1.0 km 0.5 km in the $x-$ and $z-$ directions, respectively. We set μ = 0.5, f = 500000, and τ = 0.01. The geometric elements (e_1 to e_5 in Figure 5b) were introduced to produce an estimated source close to Bott and Scott's (1964) interpretation. Elements e_1 to e_3 have a target density contrast of –0.16 g/cm^3, and elements e_4 and e_5 were assigned target density contrasts of –0.13 g/cm^3 and –0.10 g/cm^3, respectively. The result is shown in Figure 5b, which is very close to Bott and Scott's (1964) interpretation, but displaying a better anomaly fit as shown in Figure 5a (solid black line).

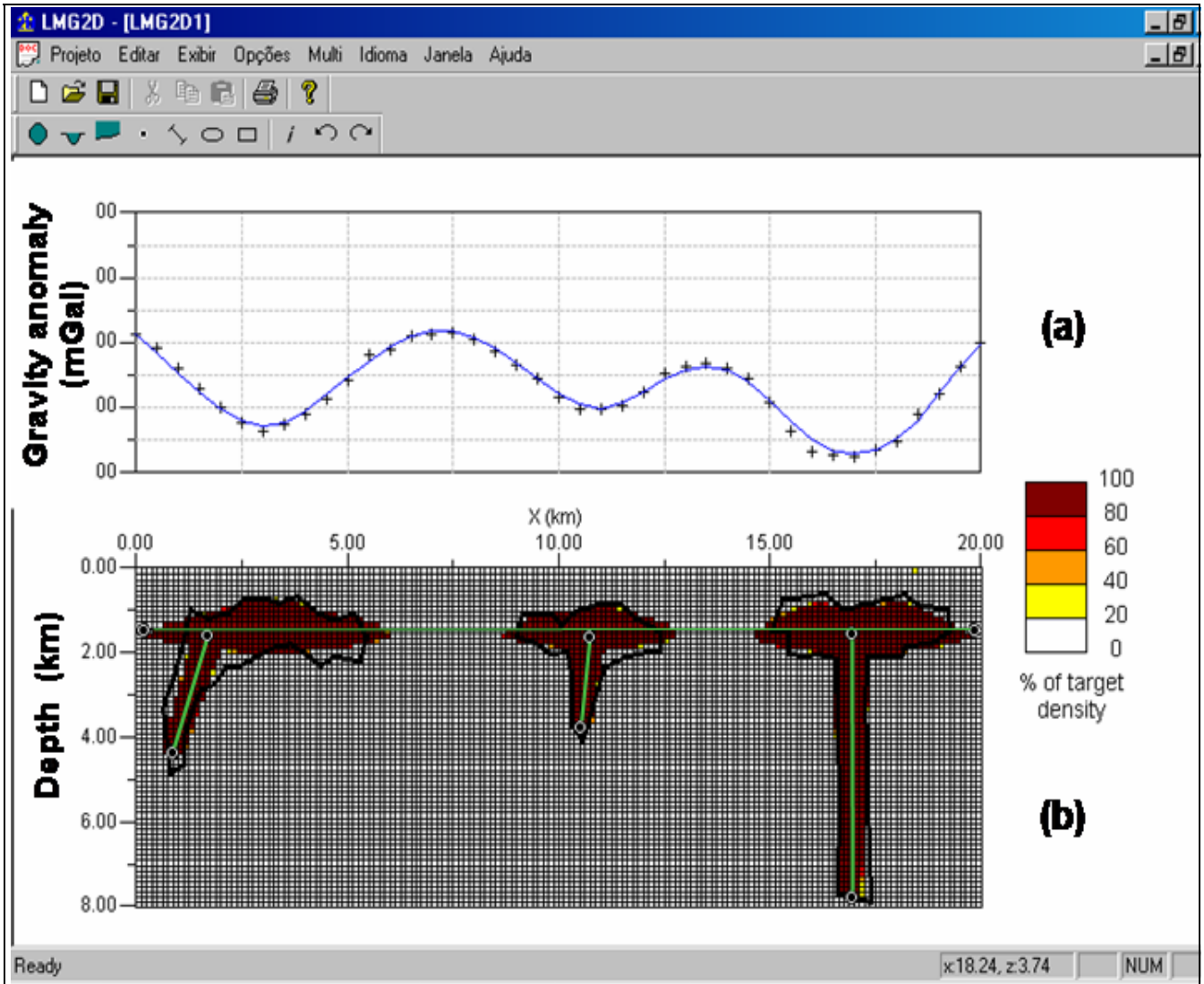

Figure 2 - Synthetic example simulating complex and laterally interfering sources. (a) Noise-corrupted Bouguer (crosses) and fitted (solid blue line) anomalies. (b) Simulated salt canopies (solid black thick lines) having density contrast of –0.2 g/cm3 and inversion result (colored cells) using four presumably known axes (green lines).

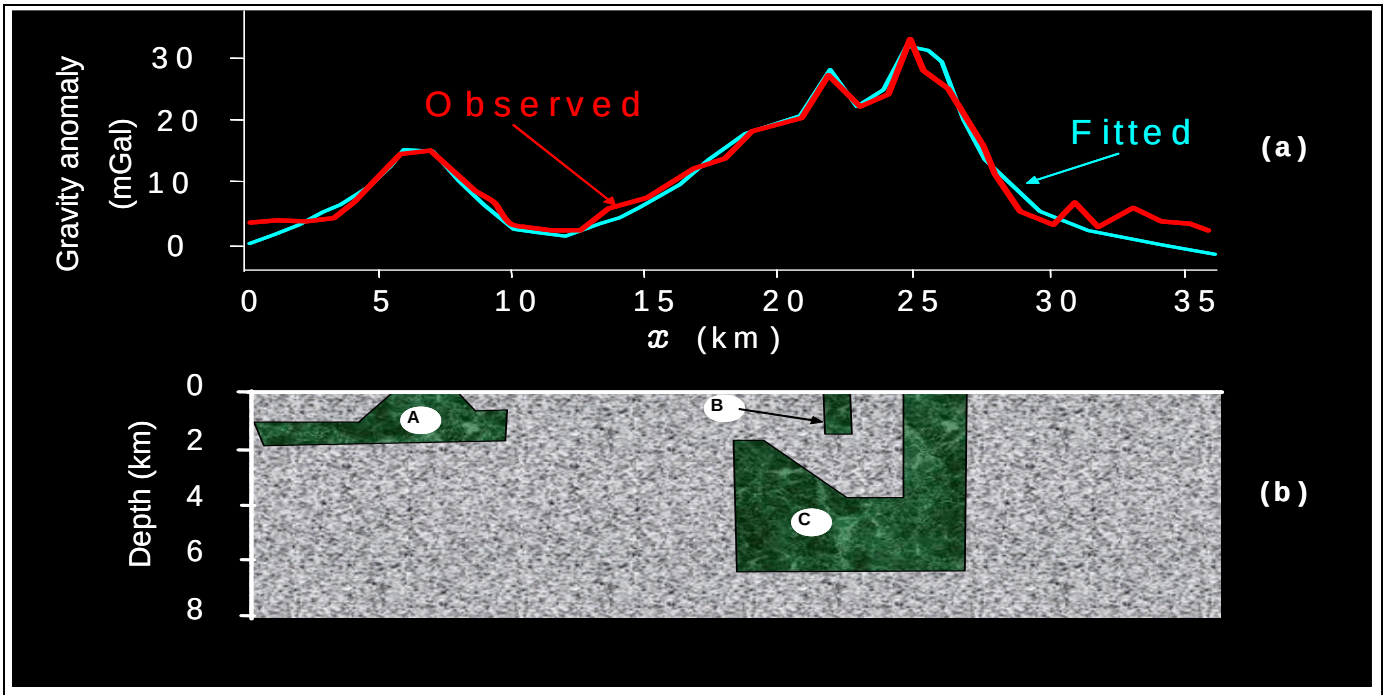

Figure 3 - Rio Maria greenstone belt. (a) Observed (red line) and fitted (blue line) Bouguer anomalies. (b) Interactive modeling (green polygons) according to Souza et al. (1992), assigning uniform density contrasts of 0.3 g/cm^3, 0.32 g/cm^3, and 0.32 g/cm^3 to sources A, B, and C, respectively.

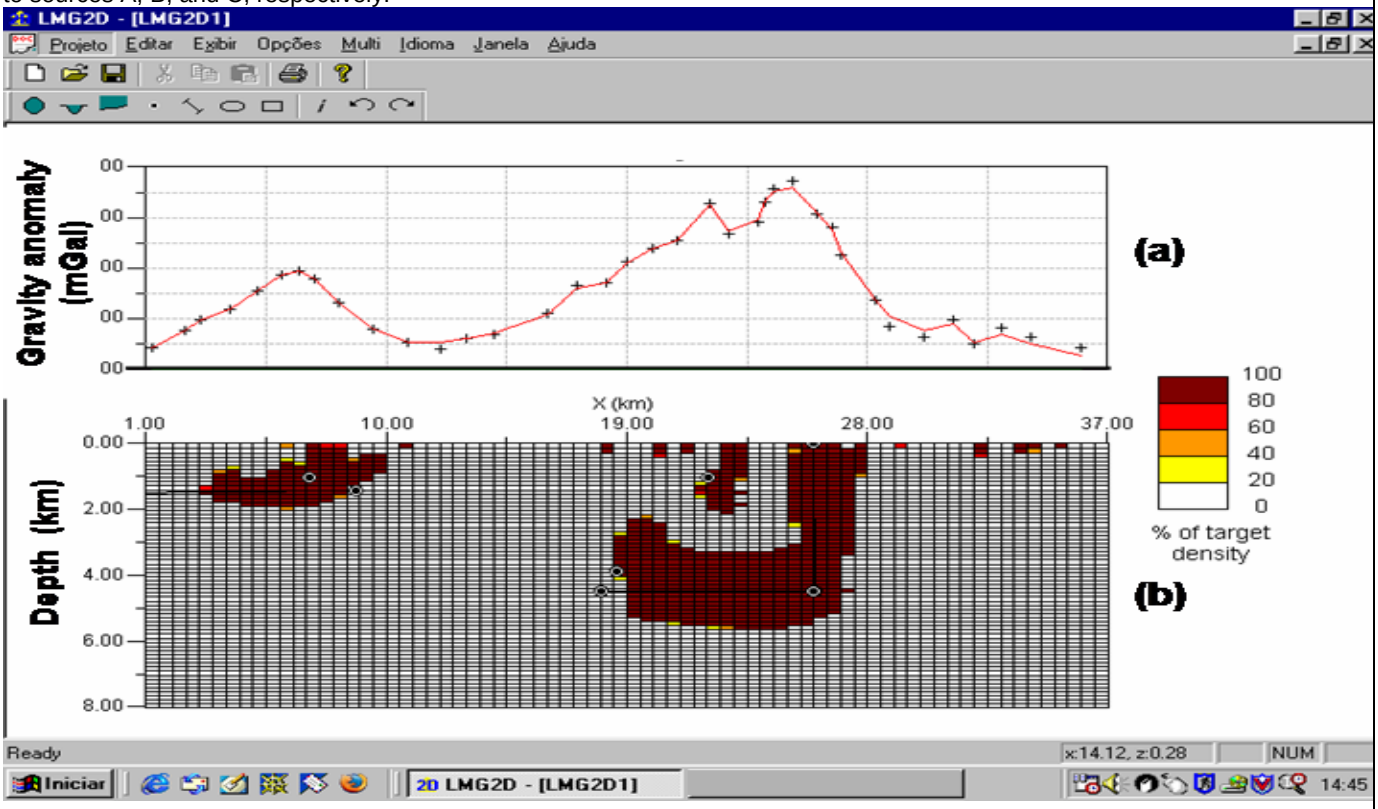

Figure 4 - Rio Maria greenstone belt. (a) Observed (crosses) and fitted (red line) Bouguer anomalies. (b) Inversion result using the present method (collored cells) and assigning a single target density contrast of 0.3 g/cm3 to axes (black lines) and to points (dots) .

Conclusions

We have proposed a new approach for delineating 2D gravity sources on the $x-z$ plane, which is similar to interactive modeling but differs from it in automatically fitting the observations and in requiring from the interpreter only the knowledge of the outlines of the sources expressed by simple geometric elements such as points and line segments. In other words, the proposed inversion method relieves the interpreter from the tedious data fitting procedure by trial-and-error, which requires trying a large number of geometries to obtain an acceptable data fit. Rather, it requires just an interactive definition of a few geometric elements defining the source's framework. Tests with synthetic and real data indicate the potential practical utility of the method in interpreting anomalies from geological settings consisting of multiple and interfering sources with complex geometry, where automatic inversion methods are prone to fail. Despite being a step forward in allowing more complex interpretations than automatic inversions, the presented method must be further improved to allow interpretations of much more complex geological settings, as for example, sedimentary environments with several faulted and folded layers and intrusive structures. Extensions to 3D and magnetic sources present no difficulty in the inversion methodology. If the method is to be implemented in a user-friendly graphical environment, however, the difficulty in the 3D extension comprises *i*) the visualization of the estimated sources and *ii*) the interactive definition of the 3D geometric elements positions in a 2D screen.

References

Bott, M. H. P., and P. Scott, 1964, Recent geophysical studies in south-west England, *in* Hosking, K.F.G., and Shrimpton, G.J., Eds., Present view of some aspects of the geology of Cornwall, Blackford, Truro: Royal Geological Society of Cornwall. 25- 44.

Guillen, A., and V. Menichetti, 1984, Gravity and magnetic inversion with minimization of a specific functional: Geophysics, 49, 1354-1360.

Souza, Z. S., J. G. Luiz, J. C. R. Cruz, and R. N. Paiva, 1992, Geometry of Archaean greenstone belts from Rio Maria (SW Pará province, Brasil) (in portuguese): Revista Brasileira de Geociências, 22, 198-203.

Acknowledgments

We thank Dr. Yonghe Sun, Dr. John Peirce, Dr. Mark Pilkington and Dr. John Bain for their questions and suggestions that greatly improved the original text. This study was supported by the CTMINERAL grant by CNPq under contract No. 505265/2004-4. The authors were supported in this research by fellowships from Conselho Nacional de Desenvolvimento Científico e Tecnológico (CNPq), Brazil. Additional support for the authors was provided by CNPq under contract No. 504419/2004-8. One of the authors (V.C.F.B.) was also supported by CNPq (contract No. 472229/03-6) and by CNPq/FAPERJ (contract No. E-26/170.733/2004).

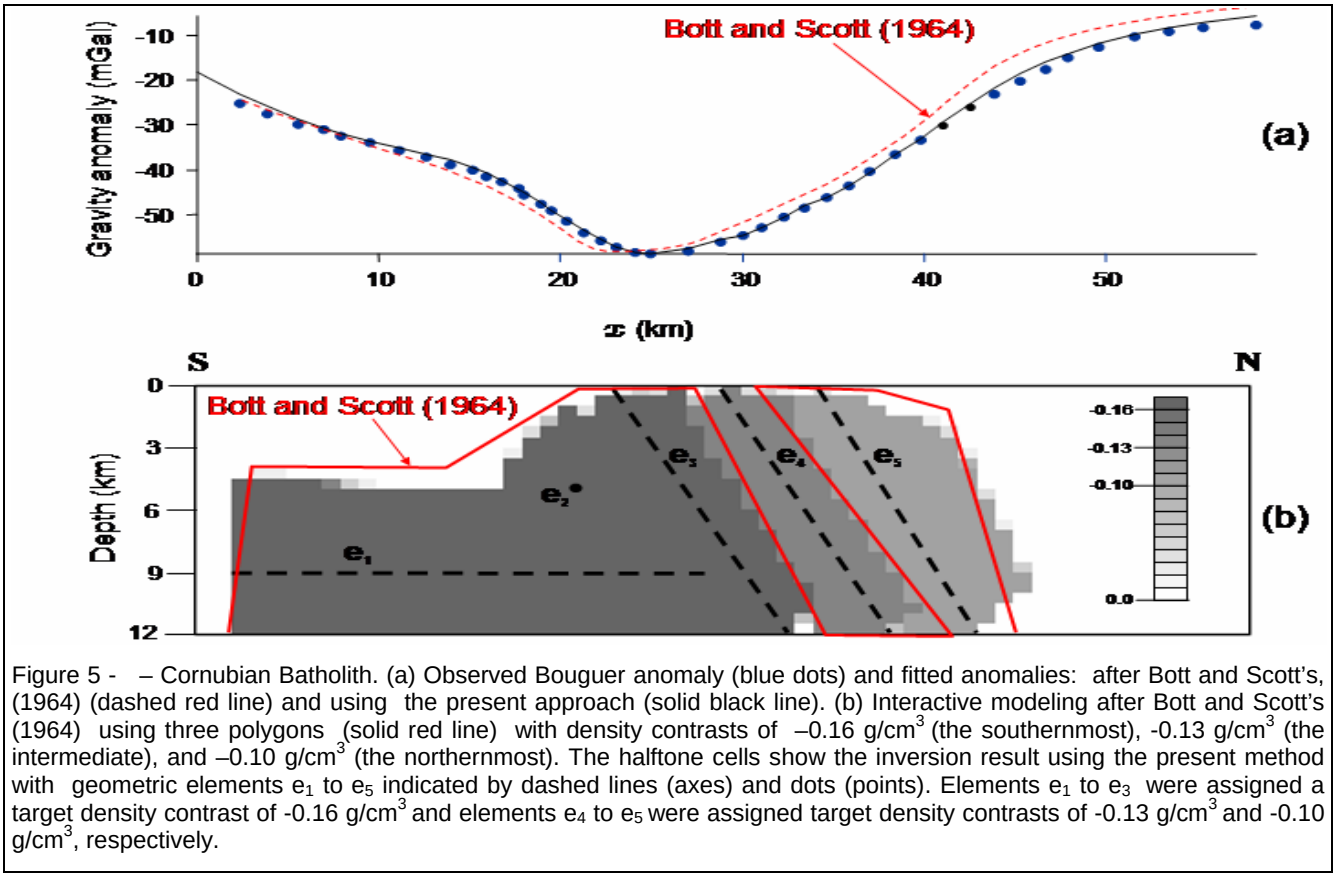

Figure 5 - – Cornubian Batholith. (a) Observed Bouguer anomaly (blue dots) and fitted anomalies: after Bott and Scott's, (1964) (dashed red line) and using the present approach (solid black line). (b) Interactive modeling after Bott and Scott's (1964) using three polygons (solid red line) with density contrasts of –0.16 g/cm^3 (the southernmost), -0.13 g/cm^3 (the intermediate), and –0.10 g/cm^3 (the northernmost). The halftone cells show the inversion result using the present method with geometric elements e_1 to e_5 indicated by dashed lines (axes) and dots (points). Elements e_1 to e_3 were assigned a target density contrast of -0.16 g/cm^3 and elements e_4 to e_5 were assigned target density contrasts of -0.13 g/cm^3 and -0.10 g/cm^3, respectively.